Fabrication of monolithic microfluidic channels in diamond with ion beam lithography

FABRICATION OF MONOLITHIC MICROFLUIDIC CHANNELS IN DIAMOND WITH ION BEAM LITHOGRAPHY

F. Picollo[1,2,3,4], A. Battiato[1,2,3,4], L. Boarino[5], S. Ditalia[1,2,3,4], E. Enrico[5], J. Forneris[1,2,3,4], A. Gilardino[6,3], M. Jakšić[7], F. Sardi[1], N. Skukan[7], A. Tengattini[1,2,3,4], P. Olivero[1,2,3,4], A. Re[1,2,3,4], E. Vittone[1,2,3,4]

[1] Physics Department, University of Torino, Torino, Italy

[2] Istituto Nazionale di Fisica Nucleare (INFN), Sezione di Torino, Torino, Italy

[3] "NIS" Inter-departmental Centre, University of Torino, Torino, Italy

[4] Consorzio Nazionale Inter-universitario per le Scienze fisiche della Materia (CNISM), Sezione di Torino, Torino, Italy

[5] Nanofacility Piemonte, National Institute of Metrologic Research (INRiM), Torino, Italy

[6] Department Of Life Sciences And Systems Biology, University of Torino, 10123 Torino, Italy

[7] Laboratory for Ion Beam Interactions, Ruđer Bošković Institute, Zagreb, Croatia

Keywords: Deep ion beam lithography, diamond, microfluidic, fluorescent imaging

NUM PAG

ABSTRACT

In the present work, we report on the monolithic fabrication by means of ion beam lithography of hollow micro-channels within a diamond substrate, to be employed for microfluidic applications.

The fabrication strategy takes advantage of ion beam induced damage to convert diamond into graphite, which is characterized by a higher reactivity to oxidative etching with respect

to the chemically inert pristine structure. This phase transition occurs in sub-superficial layers thanks to the peculiar damage profile of MeV ions, which mostly damage the target material at their end of range.

The structures were obtained by irradiating commercial CVD diamond samples with a micrometric collimated C^+ ion beam at three different energies (4 MeV, 3.5 MeV and 3 MeV) at a total fluence of 2×10^{16} cm^{-2}. The chosen multiple-energy implantation strategy allows to obtain a thick box-like highly damaged region ranging from 1.6 μm to 2.1 μm below the sample surface. High-temperature annealing was performed to both promote the graphitization of the ion-induced amorphous layer and to recover the pristine crystalline structure in the cap layer. Finally, the graphite was removed by electrochemical etching, obtaining monolithic microfluidic structures.

These prototypal microfluidic devices were tested injecting aqueous solutions and the evidence of the passage of fluids through the channels was confirmed by confocal fluorescent microscopy.

1. Introduction

'Lab-on-a-chip' technology is an emerging field exploited for a wide range of applications. The benefits of these platforms for the study of biological systems or chemical reactions have been widely reviewed in previous works [1–6]. Microfluidic lab-on-a-chips consist of small devices equipped with channel having size in the range of micrometres, which facilitates handling of volumes below the microliter range.

Microfluidic systems can be integrated with analytical detection techniques [7,8], such as electrochemical and optical methods including absorption, chemoluminescence and fluores-

cence. Moreover, they can be employed in biosensing devices both as active component for cell activity monitoring [9–11] or as perfusion system for drug/solution transport [12].

The vast majority of microfluidic devices consist, however, of simple planar microchips fabricated by photolithography on standard substrates such as glass, silicon or polymers.

The employment of diamond as a substrate material would represent a significant improvement for specific applications in this research field since it guarantees to the final device high chemical inertness, mechanical stability, wide transparency window from IR to near UV and long term biocompatibility [13,14]. To this scope, the fabrication of microfluidic structures in diamond has already been explored with standard lithographic techniques, for which the definition of three-dimensional structures typically requires multiple processing steps in non-monolithic polycrystalline substrates [15–17]. Deep Ion Beam Lithography (DIBL) represents a versatile fabrication tool for the structural modification of diamond [18,19], with significant applications in the realization different types of integrated devices, as already demonstrated in previous works [20–22]. In particular, the use of DIBL for the fabrication of thin microfluidic structures was preliminary explored by M. A. Strack et al. with a single-energy ion implantation strategy [23].

In the present paper, we report on the employment of a three-dimensional lithographic technique based on multiple-energy collimated MeV ion beams for the realization of thick monolithic microfluidic structures in diamond.

2. Experimental

The sample under analysis consists of an artificial single-crystal diamond grown by chemical vapor deposition (CVD) by ElementSix. The diamond is 3×3×0.5 mm^3 in size and it is classified as type IIa ("optical grade") with a concentration of substitutional nitrogen lower than

1 ppm. The sample is cut along the 100 crystal direction and it is optically polished on the two large opposite faces.

The diamond was implanted with a collimated MeV C^+ ion beam at room temperature at the Laboratory for Ion Beam Interaction of the Ruđer Bošković Institute (LIBI-RBI).

The high damage density produced by ion implantation, which occurs mainly at ion end of range in correspondence of the Bragg-peak, promotes the conversion of the diamond lattice into an amorphous phase once a critical damage density threshold is overcome [24–26]. Thermal treatment (950 °C for 2 hours, in this study) induces the transition of this modified region to polycrystalline graphite, which represents the thermodynamically stabile allotropic form of carbon [27,28]. The thickness of this graphitic layer is determined by the ion damage profile and usually ranges from 100 nm to 250 nm, depending on the implantation parameters.

With the purpose of creating channels with appropriate thicknesses (i.e. significantly larger than the above-mentioned values) for applications in micro-fluidics, a multiple-energy implantation approach was adopted instead a single-energy implantation [23]. Carbon ions with three different decreasing energies (i.e.: 4 MeV, 3.5 MeV and 3 MeV) were employed, by suitably tuning the respective fluences (i.e.: 2×10^{16} ion cm^{-2} for the former energy and 1.2×10^{16} ion cm^{-2} for the latter ones) in order to have a uniform "box-like" above-threshold damage density profile. Particularly, the energies chosen guarantee the creation of a buried graphitic layer at 1.6 μm below the surface having an overall thickness of ~500 nm, as confirmed by the SRIM Monte Carlo [29] simulation reported in Fig. 1.

The implantation was performed using a collimated ion beam [30] obtained by employing a metal mask which guarantees the control of the structures geometry with micrometric spatial resolution (see the schematics in Fig. 1). The thickness of the collimator element is defined to fully stop the incoming ions with the highest energy. This approach allows to per-

form multiple-energy irradiation of the desired region while avoiding beam refocusing and beam sample drift or misalignments during the required implantation times.

The obtained graphitic structures were fully embedded into the diamond matrix. Thus, Focused Ion Beam milling was necessary to create access holes to expose their endpoints to the external environment. This post-processing step was performed with a Quanta 3D™ dual-beam system by FEI, available at the "NanoFacility Piemonte" laboratories of the Italian National Institute of Metrological Research (INRiM), employing 30 keV Ga^+ focused-ion-beam with the possibility to progressively monitor sample modification by means of SEM imaging.

The creation of hollow microfluidic channels was finalized by the selective removal of the graphite with respect to the surrounding diamond matrix, using high-temperature ozone etching. The set-up employed consists of an annealing chamber equipped with ultraviolet lamp (emission peak at 184.9 nm) and an oxygen injection system. UV irradiation of the sample was carried out exploiting a sapphire window, which is transparent in the required spectral range for the ozone production in the chamber. The sample was exposed to ozone environment at a pressure of 800 mbar at a temperature of 450 °C. The duration of the process is strictly dependent on the structures geometry (i.e. length, thickness, extension of the FIB holes, ...) ranging from 10 to 50 hours.

The employed process take advantage of the high reactivity of ozone that can oxidize carbon with the subsequent production of carbon oxide or carbon dioxide. The selective etching of graphite is obtained in a temperature range of 370 – 500 °C, while for higher values also diamond would be oxidized.

Figure 2 shown the progressive removal of a test structure after increasing etching times (i.e. 0, 6, 36, 42 hours): at the end of the process, the hollow microfluidic channels are still barely

visible thanks to a residual optical contrast due multiple internal reflections at the air/diamond interfaces.

Scanning Electron Microscopy (SEM) was employed to confirm the predicted geometry of the channels, in terms of thicknesses of both the cap layer and the etched region, as reported in Fig. 1.

The functionality of the microfluidic devices was tested by optical microscopy (both in transmission and confocal luminescence) of different injected fluids.

Confocal luminescence images (1024 × 1024 pixels, 16-bit gray scale) were acquired using a Fluoview 200 laser scanning confocal microscope (Olympus America Inc., Melville, NY, USA) equipped with a monochromator system attached to an inverted microscope with 50× and 60× objectives [31]. Two different excitation wavelengths (i.e. 568 nm and 488 nm) were simultaneously employed to selectively stimulate the fluorescence emission from either the injected Fluorescein dye and the luminescence background of the diamond substrate. The latter luminescence signal mainly arises from the nitrogen-vacancy NV centers [32] formed in the cap layer during the fabrication process. Confocal micrographs were acquired using an enhanced CCD Camera (PCO) and the Metafluor Software (Universal Imaging Co.), and subsequent 3D optical sectioning was performed to confirm the presence of the fluid into the micro-channels. Image processing was performed using the ImageJ software [33]with the Fuji plug-in [34].

3. Results

Figure 3 shows a sequence of transmission optical micrographs highlighting the diffusion of an aqueous solution containing black dye in the microfluidic channel. A small drop of solution was delivered in proximity of one of the access endpoints and the liquid penetration

was driven by capillary forces. The images sequence was obtained capturing few frames from the video reported in the "supporting information" of the paper (video_1).

Confocal microscopy was performed in order to have a further confirmation of the presence of the liquid inside the fabricated structures.

As mentioned above, the defective structure in the cap layer of the diamond sample hosts nitrogen-vacancy (NV) fluorescent complexes in high concentrations, which exhibit a bright red emission (~690 nm) if stimulated with green light (~550 nm).

It was therefore necessary to choose a fluorophore which excitation/emission features which do not overlap with the ones of the NV center. Fluorescein isothiocyanate (FITC) fulfills this requirement, having an emission peak at ~525 nm and excitation wavelength of ~480 nm.

Figure 4 shows the optical sectioning of a microfluidic channel fill of a 1 μM FITC solution. Four optical sections are reported at increasing depth from the surface (i.e., respectively 0 μm, -1.8 μm, -2.0 μm and -3.2 μm), as schematically represented in fig. 4a. The first (0 μm) and the last (-3.2 μm) stack are characterized by the absence of FITC signal and a different intensity of red emission: as expected, residual damage induced by ion implantation increases the density of NV centers in the cap layer, while the bulk material exhibits a weak emission due to intrinsic defects. On the other hand, the intermediate (i.e. -1.8 μm and -2.0 μm, corresponding to the inner part of the microfluidic channel as previously indicated in the SEM image of Fig. 1) stacks show an intense green luminescence, related to the injected FITC solution, which is visible especially in correspondence of the liquid meniscus.

Finally, the optical cross-section of a 3D reconstructed confocal image gives a further evidence of the presence of the luminescent dye inside the microfluidic structure (see fig. 4c): the green emission from the FITC is clearly included between the cap layer and the bottom of the channel.

4. Conclusions

In the present paper, we reported on the realization of monolithic microfluidic channels in diamond by means of a lithographic technique based on the use of multiple-energy collimated MeV ions.

Optical transmission and confocal luminescence microscopies have confirmed the injection of fluids inside the realized microfluidic structures.

The reported strategy represents a useful tool to realize innovative lab-on-a-chip devices allowing for "extreme" microfluidics, i.e. experiments involving the use of highly corrosive fluids and/or high-temperature chemical reactions, thus taking advantage of the unique chemical and physical properties of the diamond substrate (chemical inertness, thermal conductivity) combined with a wide optical transparency.

Acknowledgements

This work is supported by the following projects: "DiNaMo" (young researcher grant, project n° 157660) by the Italian National Institute of Nuclear Physics; FIRB "Futuro in Ricerca 2010" project (CUP code: D11J11000450001) funded by the Italian Ministry for Teaching, University and Research (MIUR); "A.Di.N-Tech." project (CUP code: D15E13000130003) funded by the University of Torino and "Compagnia di San Paolo" and Italian MIUR (PRIN 2010/2011 project 2010JFYFY2). "Nanofacility Piemonte" is a laboratory at INRiM supported by the "Compagnia di San Paolo" Foundation.

References

[1] P.S. Dittrich, A. Manz, Lab-on-a-chip: microfluidics in drug discovery., Nat. Rev. Drug Discov. 5 (2006) 210–218. doi:10.1038/nrd1985.

[2] Y. Zhang, P. Ozdemir, Microfluidic DNA amplification-A review, Anal. Chim. Acta. 638 (2009) 115–125. doi:10.1016/j.aca.2009.02.038.

[3] C.-Y. Lee, C.-L. Chang, Y.-N. Wang, L.-M. Fu, Microfluidic mixing: a review., Int. J. Mol. Sci. 12 (2011) 3263–87. doi:10.3390/ijms12053263.

[4] P. Abgrall, A.-M. Gué, Lab-on-chip technologies: making a microfluidic network and coupling it into a complete microsystem—a review, J. Micromechanics Microengineering. 17 (2007) R15–R49. doi:10.1088/0960-1317/17/5/R01.

[5] X. Chen, Topology optimization of microfluidics - A review, Microchem. J. 127 (2016) 52–61. doi:10.1016/j.microc.2016.02.005.

[6] R. Konwarh, P. Gupta, B.B. Mandal, Silk-microfluidics for advanced biotechnological applications: A progressive review, Biotechnol. Adv. 34 (2016) 845–858. doi:10.1016/j.biotechadv.2016.05.001.

[7] J. Wu, M. Gu, Microfluidic sensing: state of the art fabrication and detection techniques., J. Biomed. Opt. 16 (2011) 080901. doi:10.1117/1.3607430.

[8] E. Verpoorte, Microfluidic chips for clinical and forensic analysis, Electrophoresis. 23 (2002) 677–712. doi:10.1002/1522-2683(200203)23:5<677::AID-ELPS677>3.0.CO;2-8.

[9] Y. Gao, S. Bhattacharya, X. Chen, S. Barizuddin, S. Gangopadhyay, K.D. Gillis, A microfluidic cell trap device for automated measurement of quantal catecholamine release from cells., Lab Chip. 9 (2009) 3442–3446. doi:10.1039/b913216c.

[10] C. Liberale, G. Cojoc, F. Bragheri, P. Minzioni, G. Perozziello, R. La Rocca, et al., Integrated microfluidic device for single-cell trapping and spectroscopy, Sci. Rep. 3

(2013) 1–6. doi:10.1038/srep01258.

[11] J. Nilsson, M. Evander, B. Hammarström, T. Laurell, Review of cell and particle trapping in microfluidic systems, Anal. Chim. Acta. 649 (2009) 141–157. doi:10.1016/j.aca.2009.07.017.

[12] L. Kim, Y.-C. Toh, J. Voldman, H. Yu, A practical guide to microfluidic perfusion culture of adherent mammalian cells, Lab Chip. 7 (2007) 681–694. doi:10.1039/B704602B.

[13] P.A. Nistor, P.W. May, F. Tamagnini, A.D. Randall, M.A. Caldwell, Long-term culture of pluripotent stem-cell-derived human neurons on diamond – A substrate for neurodegeneration research and therapy, Biomaterials. 61 (2015) 139–149. doi:10.1016/j.biomaterials.2015.04.050.

[14] F. Picollo, A. Battiato, E. Bernardi, A. Marcantoni, A. Pasquarelli, E. Carbone, et al., Microelectrode arrays of diamond-insulated graphitic channels for real-time detection of exocytotic events from cultured chromaffin cells and slices of adrenal glands., Anal. Chem. (2016). doi:10.1021/acs.analchem.5b04449.

[15] R. Müller, P. Schmid, A. Munding, R. Gronmaier, E. Kohn, Elements for surface microfluidics in diamond, Diam. Relat. Mater. 13 (2004) 780–784. doi:10.1016/j.diamond.2003.11.097.

[16] H. Björkman, C. Ericson, S. Hjertén, K. Hjort, Diamond microchips for fast chromatography of proteins, Sensors Actuators B Chem. 79 (2001) 71–77. doi:10.1016/S0925-4005(01)00837-1.

[17] H. Björkman, P. Rangsten, P. Hollman, K. Hjort, Diamond replicas from microstructured silicon masters, Sensors Actuators A Phys. 73 (1999) 24–29. doi:10.1016/S0924-4247(98)00250-7.

[18] F. Bosia, N. Argiolas, M. Bazzan, B. a Fairchild, a D. Greentree, D.W.M. Lau, et al., Direct measurement and modelling of internal strains in ion-implanted diamond., J. Phys. Condens. Matter. 25 (2013) 385403. doi:10.1088/0953-8984/25/38/385403.

[19] F. Bosia, N. Argiolas, M. Bazzan, P. Olivero, F. Picollo, a. Sordini, et al., Modification of the structure of diamond with MeV ion implantation, Diam. Relat. Mater. 20 (2011) 774–778. doi:10.1016/j.diamond.2011.03.025.

[20] F. Picollo, A. Battiato, E. Carbone, L. Croin, E. Enrico, J. Forneris, et al., Development and Characterization of a Diamond-Insulated Graphitic Multi Electrode Array Realized with Ion Beam Lithography, Sensors. 15 (2014) 515–528. doi:10.3390/s150100515.

[21] J. Forneris, V. Grilj, M. Jakšić, a. Lo Giudice, P. Olivero, F. Picollo, et al., IBIC characterization of an ion-beam-micromachined multi-electrode diamond detector, Nucl. Instruments Methods Phys. Res. Sect. B Beam Interact. with Mater. Atoms. 306 (2013) 181–185. doi:10.1016/j.nimb.2012.12.056.

[22] F. Picollo, A. Battiato, E. Bernardi, L. Boarino, E. Enrico, J. Forneris, et al., Realization of a diamond based high density multi electrode array by means of Deep Ion Beam Lithography, Nucl. Instruments Methods Phys. Res. Sect. B Beam Interact. with Mater. Atoms. 348 (2015) 199–202. doi:10.1016/j.nimb.2014.11.119.

[23] M. a. Strack, B. a. Fairchild, A.D.C. Alves, P. Senn, B.C. Gibson, S. Prawer, et al., Buried picolitre fluidic channels in single-crystal diamond, 8923 (2013) 89232X. doi:10.1117/12.2035099.

[24] A. Battiato, M. Lorusso, E. Bernardi, F. Picollo, F. Bosia, D. Ugues, et al., Softening the ultra-stiff: Controlled variation of Young's modulus in single-crystal diamond by ion implantation, Acta Mater. 116 (2016) 95–103. doi:10.1016/j.actamat.2016.06.019.

[25] C. Uzansaguy, C. Cytermann, R. Brener, V. Richter, M. Shaanan, R. Kalish, Damage Threshold for Ion-Beam-Induced Graphitization of Diamond, Appl. Phys. Lett. 67 (1995) 1194–1196.

[26] J.O. Orwa, K.W. Nugent, D.N. Jamieson, S. Prawer, Raman investigation of damage caused by deep ion implantation in diamond, Phys. Rev. B - Condens. Matter Mater. Phys. 62 (2000) 5461–5472. doi:10.1103/PhysRevB.62.5461.

[27] F. Picollo, D. Gatto Monticone, P. Olivero, B. a. Fairchild, S. Rubanov, S. Prawer, et al., Fabrication and electrical characterization of three-dimensional graphitic microchannels in single crystal diamond, New J. Phys. 14 (2012) 053011. doi:10.1088/1367-2630/14/5/053011.

[28] F. Picollo, P. Olivero, F. Bellotti, Ž. Pastuović, N. Skukan, A. Lo Giudice, et al., Formation of buried conductive micro-channels in single crystal diamond with MeV C and He implantation, Diam. Relat. Mater. 19 (2010) 466–469. doi:10.1016/j.diamond.2010.01.005.

[29] J.F. Ziegler, M.D. Ziegler, J.P. Biersack, SRIM - The stopping and range of ions in matter (2010), Nucl. Instruments Methods Phys. Res. Sect. B Beam Interact. with Mater. Atoms. 268 (2010) 1818–1823. doi:10.1016/j.nimb.2010.02.091.

[30] F. Picollo, A. Battiato, E. Bernardi, M. Plaitano, C. Franchino, S. Gosso, et al., All-carbon multi-electrode array for real-time in vitro measurements of oxidizable neurotransmitters, Sci. Rep. 6 (2016) 20682. doi:10.1038/srep20682.

[31] A. Gilardino, F. Catalano, F.A. Ruffinatti, G. Alberto, B. Nilius, S. Antoniotti, et al., Interaction of SiO2 nanoparticles with neuronal cells: Ionic mechanisms involved in the perturbation of calcium homeostasis, Int. J. Biochem. Cell Biol. 66 (2015) 101–111.

doi:10.1016/j.biocel.2015.07.012.

[32] A.M. Zaitsev, Optical Properties of Diamond, Springer Berlin Heidelberg, Berlin, Heidelberg, 2001. doi:10.1007/978-3-662-04548-0.

[33] C.A. Schneider, W.S. Rasband, K.W. Eliceiri, NIH Image to ImageJ: 25 years of image analysis, Nat Meth. 9 (2012) 671–675. http://dx.doi.org/10.1038/nmeth.2089.

[34] J. Schindelin, I. Arganda-Carreras, E. Frise, V. Kaynig, M. Longair, T. Pietzsch, et al., Fiji: an open-source platform for biological-image analysis, Nat Meth. 9 (2012) 676–682. http://dx.doi.org/10.1038/nmeth.2019.

Figures and captions

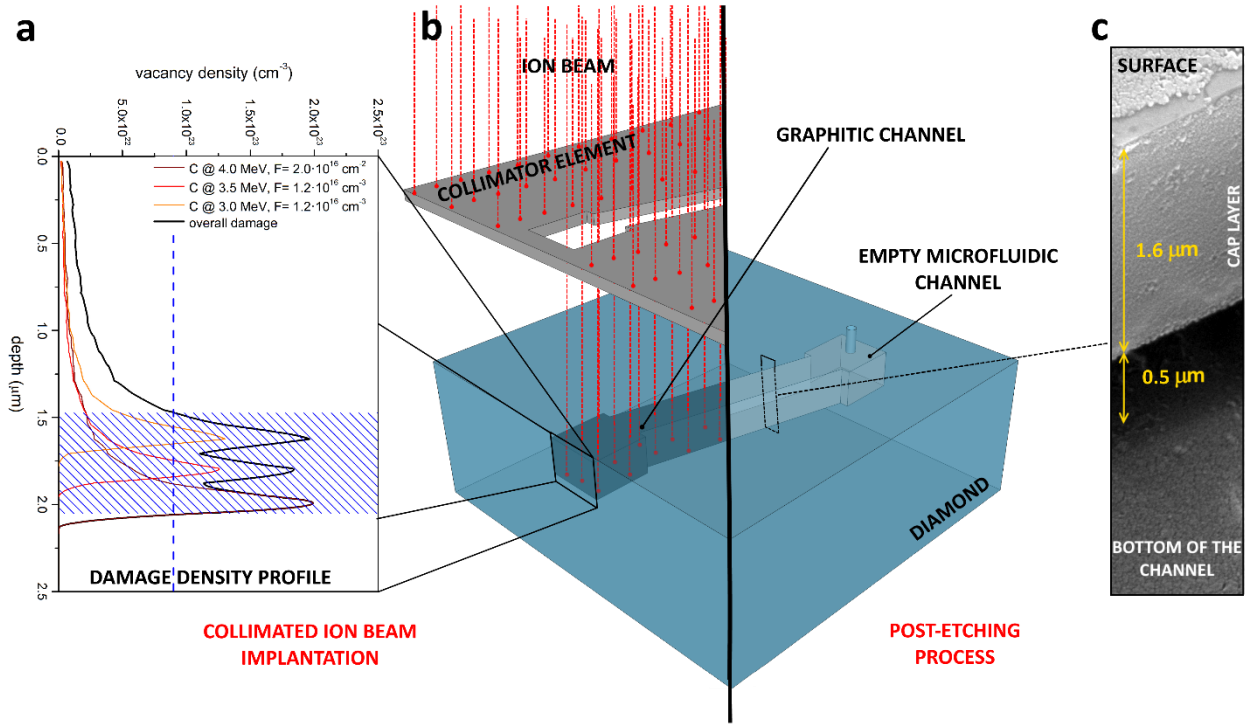

FIG 1: a) SRIM simulation of box-like implantation of C^+ ions at 4 MeV, 3.5 MeV and 3 MeV (brown, red and orange lines, respectively): the total damage (black line) and the graphitization threshold (blue dashed line) are also reported; the region where the threshold is overcome is highlighted (blue lined area). b) Schematics of collimated beam implantation process and microfluidic channel obtained after etching treatment. c) Cross-section SEM micrograph of a microfluidic structure.

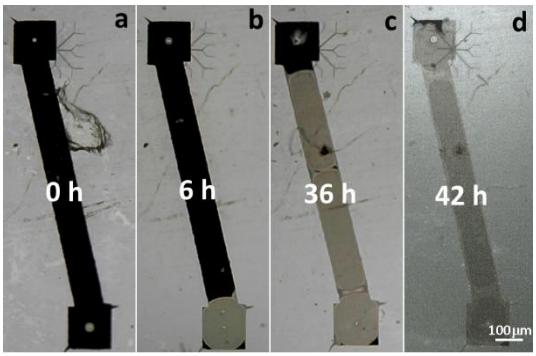

FIG 2: a-d) Series of optical micrographs showing the temporal evolution of the ozone selective removal of the graphite at 0, 6, 36 and 42 hours.

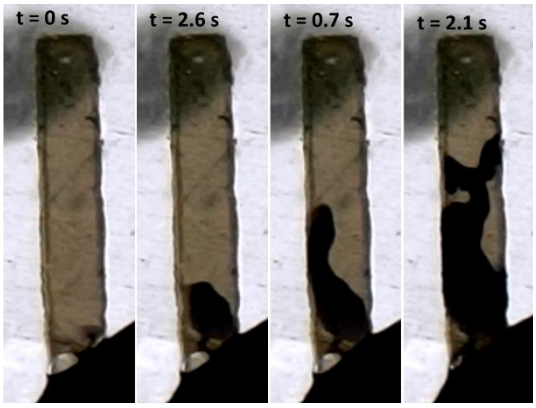

FIG 3: Sequence of video frames showing the temporal evolution of the injection of a solution containing a black dye inside a microfluidic channel.

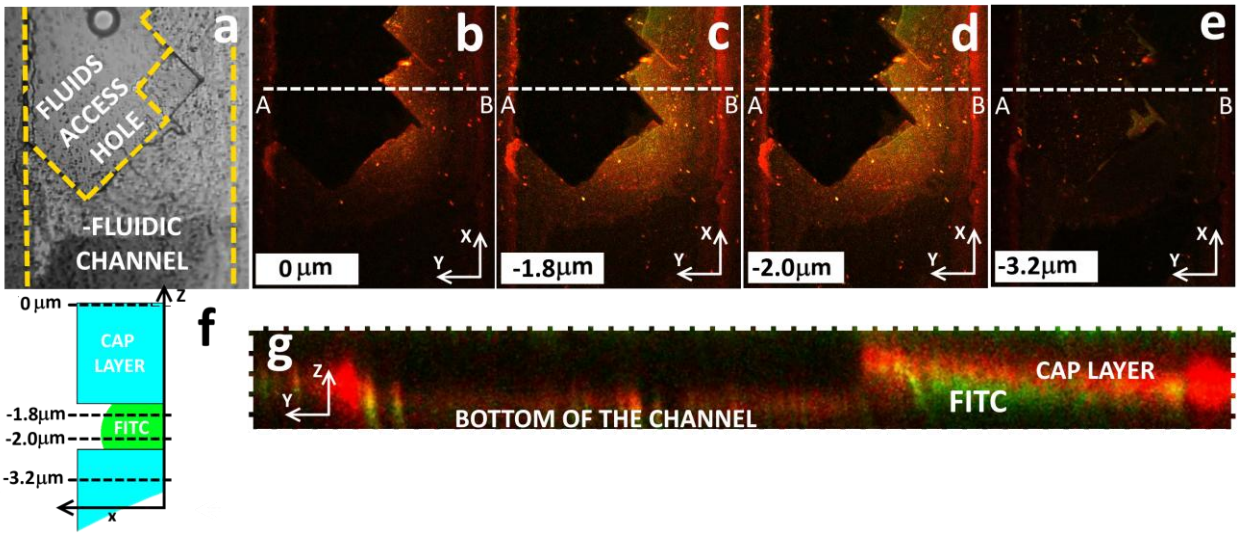

FIG 4: a) Optical transmission micrograph of the channel region under analysis: the fluid access hole is highlighted (yellow dashed line). b-e) Optical sectioning of a microfluidic channel into which a 1 µM FITC solution was injected. Four stacks in the XY plane are reported at increasing depth (Z) from the surface, i.e respectively 0 µm, -1.8 µm, -2.0 µm and -3.2 µm. f) Schematics of the stacks positions along the XZ direction of the microfluidic channel. g) Optical cross-section in the XZ plane of the 3D reconstructed image obtained along the AB line.